# Journal of Materials Chemistry C



PAPER

View Article Online



Cite this: J. Mater. Chem. C. 2023. **11**, 16316

Received 14th September 2023, Accepted 10th November 2023

DOI: 10.1039/d3tc03358a

rsc.li/materials-c

## Electronic, vibrational, and optical properties of fullerene-S<sub>8</sub> co-crystals†‡

Maliheh Shaban Tameh, D Xiaojuan Ni, D Veaceslav Coropceanu D\* and Jean-Luc Brédas \*\*

Sulfur and fullerenes are well-known materials that have received significant attention over many years and fullerene-S<sub>8</sub> co-crystals have been reported recently. Here, via density functional theory (DFT) calculations, we shed light on the electronic, vibrational, and optical properties of the  $C_{60}-2S_8$  and  $C_{70}-$ 2S<sub>8</sub> co-crystals. In both co-crystals, the holes and electrons are characterized by very small effective masses that are comparable to those derived in fullerene single crystals. Interestingly, the S<sub>8</sub> molecules are found not to contribute to charge transport as the calculations show that both types of carriers move over the networks formed by the fullerene molecules. Calculations of the excited electronic states point to the formation of charge-transfer states, where electrons are transferred from fullerene molecules to S<sub>8</sub> molecules, i.e., the fullerenes act in these co-crystals as electron donors. However, the energies of these charge-transfer states in both  $C_{60}$ – $2S_8$  and  $C_{70}$ – $2S_8$  are higher than those of several excited states localized on  $C_{60}$  or  $C_{70}$ ; therefore, the charge-transfer states play no role in the lowenergy part of the absorption spectrum. In agreement with experimental data, the calculations also show that the fullerene-S<sub>R</sub> inter-molecular interactions are very weak in the ground state; as a result, the infrared (IR) spectra of the co-crystals represent a simple superposition of the spectra of S<sub>8</sub> and fullerene molecules. Since the spectra are largely silent in the long-wave IR region (800-1250 cm<sup>-1</sup>), these fullerene-S<sub>8</sub> co-crystals are potential candidates for thermal IR imaging applications.

#### 1. Introduction

Sulfur, especially as a by-product of oil refinery, is an inexpensive and abundant material that is attracting a great deal of attention. For instance, polymers with a high sulfur content are currently used in a broad range of applications<sup>1–12</sup> including thermal IR imaging, 1,2 Li-S batteries, 3,4 repairable materials, 5,6 and environmental remediation. Elemental sulfur can be found in a variety of allotropes, 13-17 with the crown-shaped S<sub>8</sub> ring being thermodynamically the most stable form in the normal state. 18-20 S<sub>8</sub>-ring molecules form the basis for the crystal structure stable at room temperature, which is transparent in the visible. 21,22 In addition, there are many examples of compounds in which S<sub>8</sub> has been cocrystallized with a range of other molecules.<sup>23–36</sup>

The C<sub>60</sub> and C<sub>70</sub> buckminsterfullerenes also consist of a single chemical element, in this case carbon. C<sub>60</sub> and C<sub>70</sub> and their derivatives have had a significant impact on a broad range

Department of Chemistry and Biochemistry, The University of Arizona, Tucson, Arizona 85721-0041, USA. E-mail: coropceanu@arizona.edu, jlbredas@arizona.edu † This work is dedicated to the memory of Professor Gilles Horowitz, a pioneer of the field of organic electronics, a gentleman, and a mentor who inspired generations of scientists.

‡ Electronic supplementary information (ESI) available. See DOI: https://doi.org/

of applications ranging from solar cells to hydrogen gas storage, field-effect transistors, and photodetectors. 37-43 Fullerenes have been exploited as both electron donating and electron accepting materials and have been shown to display ambipolar charge transport with equivalent hole and electron mobilities.44-49

One of the first studies related to fullerene-sulfur interactions was based on C<sub>60</sub> films doped with sulfur. <sup>50</sup> The electrical conductivity of these doped films was found to increase by many orders of magnitude at high temperature, which was attributed to a donating nature of sulfur. Co-crystals containing the C<sub>60</sub> or C<sub>70</sub> fullerene and S<sub>8</sub> rings have also been of interest for many years. These systems were developed, in particular, with the hope to achieve covalent or donor-acceptor interactions between the fullerene molecules and the sulfur rings. For example,  $C_{60}$ – $2S_8$ ,  $C_{70}$ – $2S_8$ ,  $C_{70}$ – $S_8$  and  $C_{70}$ – $6S_8$  co-crystals have been synthesized and investigated. 25,26,51-59 In contrast to the sulfur-doped C<sub>60</sub> films, the conductivity measurements on these co-crystals have shown they are insulators or semiconductors.<sup>58</sup> Very recently, it was demonstrated that C<sub>60</sub>-2S<sub>8</sub> co-crystals could be used to develop cathode materials for high-performance Li-S batteries. 60 Fullerene-S8 co-crystals have also received interest with regard to the evolution of their electronic properties under high-pressure conditions.61

In spite of the broad interest raised by fullerene-S<sub>8</sub> cocrystals, a detailed description of the nature of the fullerenesulfur interactions and of their impact on the system electronic properties remains missing. In this work, we use density functional theory (DFT) calculations to shed light on the charge transport, vibrational, and optical properties of the C<sub>70</sub>-2S<sub>8</sub> and C<sub>60</sub>-2S<sub>8</sub> co-crystals. 25,52,59

## 2. Computational methodology

Density functional theory (DFT) calculations on the periodic structures of the C<sub>60</sub>-2S<sub>8</sub> and C<sub>70</sub>-2S<sub>8</sub> co-crystals were carried out using the projector-augmented wave method as implemented in the Vienna ab initio simulation package (VASP), 62-64 with the Perdew-Burke-Ernzerhof (PBE) functional and considering a Pack-Monkhorst  $\Gamma$ -centered k-point mesh of 2  $\times$  2  $\times$  2. The crystal structures were optimized by relaxing the atomic coordinates until the total force on each atom was less than 0.01 eV Å<sup>-1</sup>. Band structures and gamma-point phonon calculations were performed at the same level of theory. The infrared absorption intensities were calculated using the density functional perturbation theory approach. 65,66 The effective masses at the valence band maxima and conduction band minima were calculated through diagonalizing the  $(m_{ii}^{-1})$  tensor using a finite difference method on a five-point stencil with a 0.01 bohr<sup>-1</sup> step:

$$\frac{1}{m_{ij}} = \frac{1}{\hbar^2} \frac{\partial^2 E}{\partial k_i \partial k_j} \tag{1}$$

The hole and electron transfer integrals between adjacent molecules in the crystal were derived using a fragment orbital approach in combination with a basis set orthogonalization procedure. 67,68 These calculations were performed using the PBE and B3LYP functionals with the 6-31G(d,p) basis set. The same level of theory was also used to derive the IR vibrational spectra of the C<sub>60</sub> and C<sub>70</sub> molecules. In addition, timedependent (TD) DFT calculations at the B3LYP/6-31G(d,p) and long-range corrected LC-ωHPBE/6-31G(d,p) levels were performed to calculate the excited-state energies of C70-S8 and

C<sub>70</sub>-S<sub>8</sub> complexes extracted from the crystal structures. In the case of the LC-ωHPBE functional, the range-separation parameter,  $\omega$ , was tuned for each system following the procedure reported earlier;  $^{69}$   $\omega$  values of 0.49, 0.47, and 0.49 bohr<sup>-1</sup> were optimized for C<sub>60</sub>, C<sub>70</sub>, and S<sub>8</sub>, respectively. We considered 20% of Hartree-Fock exchange in the short range and a dielectric constant  $\varepsilon = 4$ , which is appropriate for both S<sub>8</sub> and fullerene systems. 70,71 All electronic-structure calculations on isolated molecules and molecular complexes were performed with the Gaussian 16 package.72

## Results and discussion

#### **Electronic structure**

There are four known polymorph forms of the C<sub>60</sub>-2S<sub>8</sub> cocrystal.<sup>25</sup> We focus here on the β-polymorph as it does not display any disorder of the C60 cages (hereafter, we refer to this polymorph simply as C<sub>60</sub>-2S<sub>8</sub>). C<sub>60</sub>-2S<sub>8</sub> has a P1̄ triclinic structure while  $C_{70}$ – $2S_8$  belongs to the  $P2_1/C$  monoclinic space group. 25,52 The asymmetric units of both co-crystals consist of two fullerene and four S<sub>8</sub> translationally inequivalent molecules. In both co-crystals, the S<sub>8</sub> and fullerene molecules pack in adjacent segregated stacks, see Fig. 1. The molecular stacking is along the a axis in the case of  $C_{60}$ –2S<sub>8</sub> and along the c axis in the case of  $C_{70}$ – $2S_8$ . Importantly, the intermolecular centerto-center distances between fullerene molecules are just above 1 nm, i.e., twice the van der Waals radius of the fullerenes, which points to the possibility of large electronic interactions among C<sub>60</sub> and C<sub>70</sub> molecules in these co-crystals.

The band structures of the C<sub>60</sub>-2S<sub>8</sub> and C<sub>70</sub>-2S<sub>8</sub> co-crystals obtained at the PBE level are shown in Fig. 2. The results indicate that the top of valence band (VB) and the bottom of the conduction band (CB) in both co-crystals are dominated by the fullerene wavefunctions. To understand this feature, we computed the energies of the C<sub>60</sub> and C<sub>70</sub> frontier orbitals using the same molecular geometries as those in the periodic band structure calculations. As seen from Table 1, the S<sub>8</sub> HOMO level is located about 0.7 eV lower than those of the C<sub>60</sub> and C<sub>70</sub>

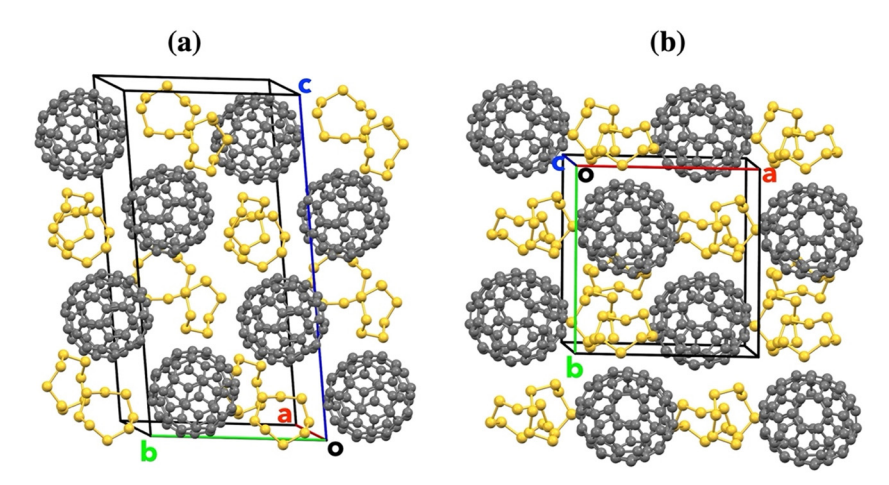


Fig. 1 Schematic representation of the crystal structures of  $C_{60}$ –2S<sub>8</sub> (a) and  $C_{70}$ –2S<sub>8</sub> (b).

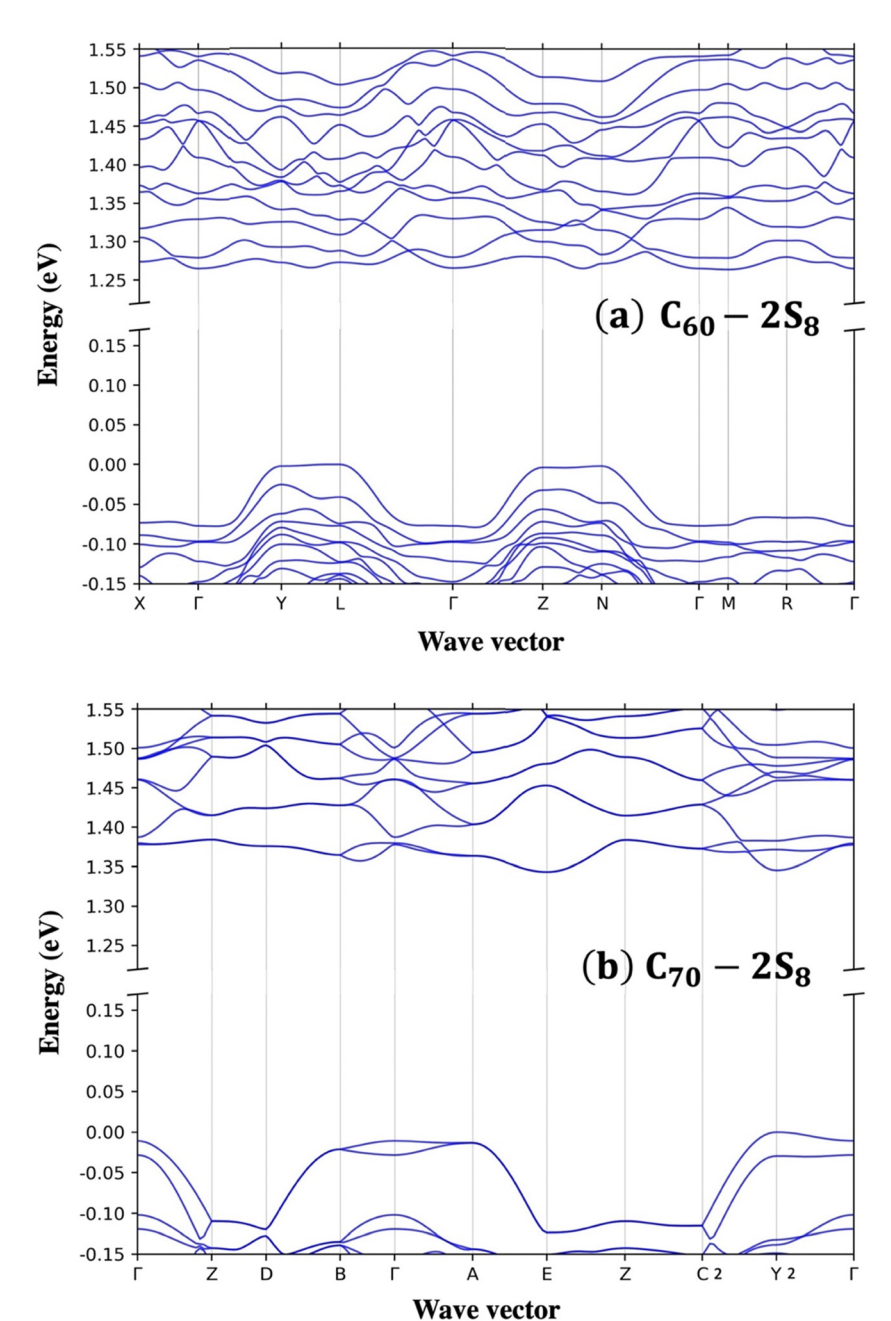


Fig. 2 (a) Electronic band structure of  $C_{60}$  –2S<sub>8</sub>. The points of high symmetry in the first Brillouin zone are labeled as follows: X = (0, -0.5, 0),  $\Gamma = (0, 0, 0)$ ,  $\Gamma = (0.5, 0.0)$ , and  $\Gamma = (0.5, 0.0)$ , and  $\Gamma = (0.5, 0.0)$ . All points are given in fractional coordinates in reciprocal space. The zero of energy is taken as the top of the VB.

**Table 1** Frontier orbital energies (in eV) of  $C_{60}$ ,  $C_{70}$ , and  $S_8$ , as calculated at the B3LYP/6-31G(d,p), PBE/6-31G(d,p), and LC- $\omega$ HPBE/6-31G(d,p) levels of theory

	B3LYP		PBE		LC-ωHPBE	
Molecule	НОМО	LUMO	НОМО	LUMO	НОМО	LUMO
C <sub>60</sub>	-5.99	-3.23	-5.50	-3.83	-6.30	-3.28
$C_{70}$	-5.91	-3.25	-5.48	-3.75	-6.23	-3.30
$S_8$	-6.66	-2.59	-6.62	-3.29	-7.75	-2.59

molecules while the  $S_8$  LUMO is found about 0.5 eV above the LUMO levels of the fullerenes. The calculations performed at the B3LYP/6-31G(d,p) and LC- $\omega$ HPBE/6-31G(d,p) levels also support this conclusion (see Table 1). We note that, here, we are interested in the relative positions of the frontier molecular levels rather than in their actual energies (which clearly depend on the choice of the functional, as seen from Table 1). The DFT calculations indicate that the electronic couplings between the  $S_8$  and fullerene frontier orbitals (see Tables S1 and S2 in the ESI‡)

Table 2 Hole and electron effective masses m (in units of the electron mass at rest,  $m_0$ ) at the band extrema of  $C_{60}$  –2S<sub>8</sub> and  $C_{70}$  –2S<sub>8</sub>

		$m/m_0$	Parallel to
C <sub>60</sub> -2S <sub>8</sub>	Holes at $\Delta_L$	1.0	a - 0.040b - 0.011c
		61.0	0.041a + b + 0.080c
		6.6	0.007a - 0.080b + c
	Electrons at $\Delta_{\Gamma}$	1.7	0.722a - 0.293b + 0.626c
	•	1.0	0.246a + 0.956b + 0.163c
		4.8	-0.646a + 0.036b + 0.762c
$C_{70}-2S_8$	Holes at $Y_2$	5.4	0.815a + 0.579c
70 0	2	1.1	b
		16.3	-0.579a + 0.815c
	Electrons at $Y_2$	2.416	a + 0.142c
	2	0.956	h
		4.464	-0.142a + c
	Electrons at E	3.520	0.997a - 0.005b + 0.077c
		3.271	0.005a + b - 0.004c
		1.681	-0.077a + 0.004b + 0.997c

do not exceed 100 meV, which points to only minor hybridization between fullerene and S<sub>8</sub> levels.

In the case of  $C_{60}$ –2S<sub>8</sub>, the VB maximum is located at  $\Delta_L$  = (0.5, -0.429, 0), *i.e.*, close to high-symmetry point L = (0.5, -0.5, -0.5, -0.5)0). As seen from Fig. 2, there is no significant band dispersion along YL and ZN, which means that there are only weak interactions between C<sub>60</sub> fullerenes along the b-axis in real space. In contrast, the valence band is more dispersive along

the  $\Gamma Y$ ,  $L\Gamma$ , and  $\Gamma Z$  k-paths, demonstrating significant coupling among C<sub>60</sub> frontier orbitals along the a-axis, i.e., along the stacking direction of the C60 molecules. This finding is consistent with the results obtained for the effective masses, see Table 2. The smallest effective hole mass, about  $\sim 1 m_0$  (where  $m_0$  is the electron mass at rest) is found indeed along the a-axis and the largest hole mass component (61  $m_0$ ) is found along the b-axis. Additional direct calculations of the transfer integrals confirm that there exists a significant electronic coupling (33 meV) along the a-axis direction (see Fig. S1 and Table S3, ESI‡).

The bottom of the CB in  $C_{60}$ –2S<sub>8</sub> has several local minima [i.e,  $\Delta_{\Gamma} = (-0.007, -0.003, 0.010), \Delta_{N} = (-0.531, -0.357, 0.578),$ and  $\Delta_M = (-0.007, -0.003, 0.010)$ ] with nearly identical energies (within 3 meV). The largest band dispersion is observed along the ΓL, ΓN, and ΓX pathways. This results into two small effective-mass components of 1  $m_0$  and 1.7  $m_0$  along the b-axis and in the ac plane, respectively. Thus, in the case of electrons, charge transport in the C<sub>60</sub>-2S<sub>8</sub> co-crystal has more of a 3D character. For the sake of comparison, we note that the effective masses for holes and electrons in the face-centeredcubic  $C_{60}$  crystal are 1.7  $m_0$  and 1.3  $m_0$ , respectively.<sup>73</sup>

The  $C_{70}$ –2S<sub>8</sub> band structure is depicted in Fig. 2b. We note that, in this co-crystal, the  $C_{70}$  molecules stack along the *c*-axis. The maximum of the VB is located at  $Y_2 = (-0.5, 0, 0)$ . The top of the VB displays moderate band dispersion along the  $ZC_2$ ,  $Y_2\Gamma$ ,

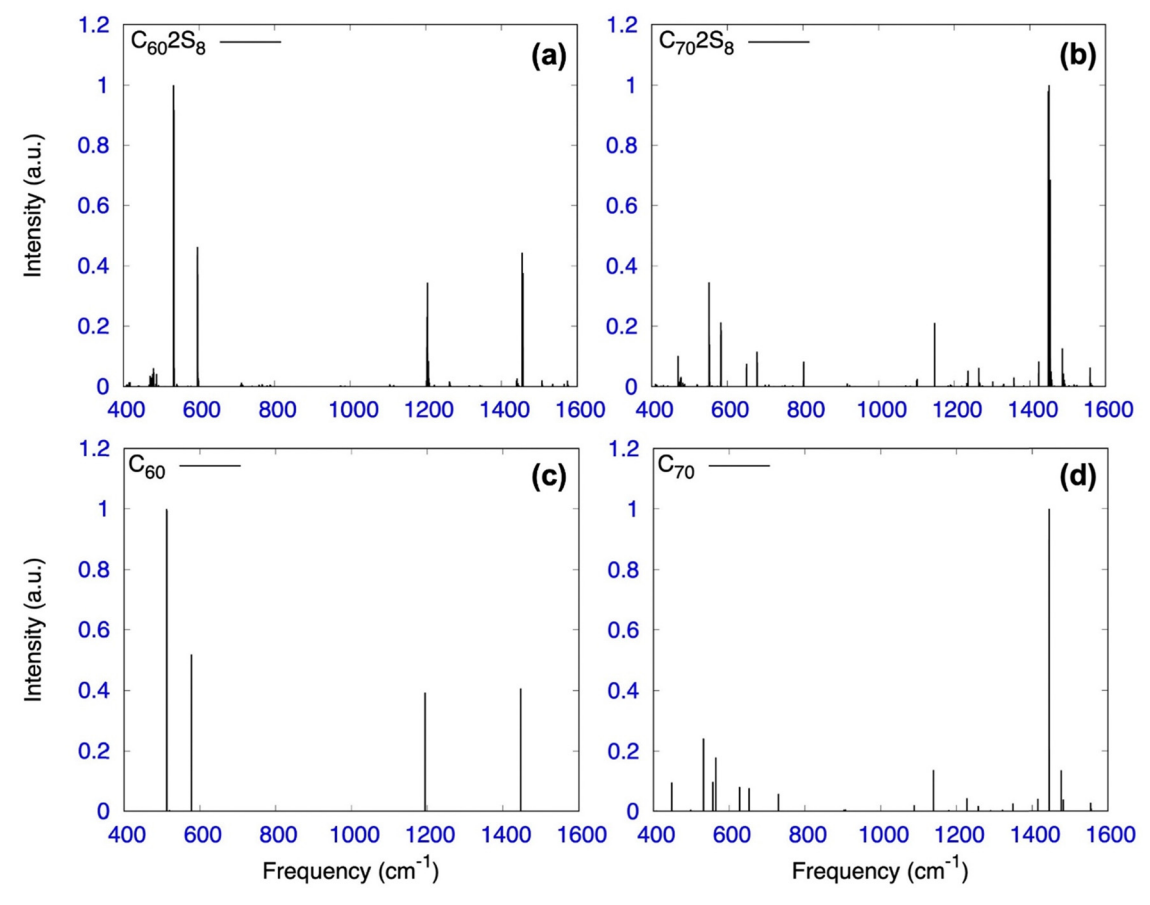


Fig. 3 IR spectra of the C<sub>60</sub>-2S<sub>8</sub> (a) and C<sub>70</sub>-2S<sub>8</sub> (b) co-crystals and IR spectra of isolated C<sub>60</sub> (c) and C<sub>70</sub> (d) molecules, as calculated at the PBE level.

**Table 3** Singlet excited-state transition energies (in eV) of the  $S_8$  and  $C_{60}$  molecules and  $S_8-C_{60}$  complex, as obtained from TD-DFT calculations at the B3LYP/6-31G(d,p) level of theory

Transition	$S_8$	$C_{60}$	$S_8 - C_{60}$
$S_0 \rightarrow S_1$	3.73	2.10	2.09
$S_0 \rightarrow S_{15}$	4.30	2.28	2.28
$S_0 \rightarrow S_{16}$	4.34	3.21	2.84

ZD, and EZ k-paths, suggesting weak interactions among  $C_{70}$  molecules along the a-axis and c-axis in real space. However, significant dispersion is observed along the  $Y_2C_2$  and AE directions, i.e., along the b-axis. The effective-mass calculations show that the smallest component for holes  $(1.7 m_0)$  is oriented indeed along the b-axis. The CB minimum is located at E = (-0.5, 0.5, 0.5). As in the case of  $C_{60}$ -2S<sub>8</sub>, the CB also displays an additional local minimum at  $Y_2 = (-0.5, 0, 0)$ , located just 2 meV above the E point. As for the holes, the smallest effective-mass component for electrons  $(1 m_0)$  is obtained along the b-axis. However, relatively small effective-mass values  $(<2 m_0)$  are also obtained for electrons moving in the ac plane, suggesting that, as in the case of  $C_{60}$ -2S<sub>8</sub>, the electrons in  $C_{70}$ -2S<sub>8</sub> display a 3D charge transport character.

#### Infrared (IR) properties

As mentioned in the Introduction, polymers with a high sulfur content have emerged as a new class of materials for IR imaging.  $^{1,74-76}$  Regions of special interest are the long-wave (LWIR, 8–12.5  $\mu$ m/800–1250 cm $^{-1}$ ) and mid-wave (MWIR, 3–5  $\mu$ m/2000–3300 cm $^{-1}$ ) IR spectral windows. Experimental data show that S<sub>8</sub> exhibits only a few weak IR transitions that are found in the range of 100–500 cm $^{-1}$ . Thus, S<sub>8</sub> is transparent in both LWIR and MWIR windows. In a recent theoretical work, we showed that the C<sub>60</sub> and C<sub>70</sub> molecules are also fully transparent in the MWIR window and highly transparent in the LWIR region. Therefore, it is interesting to investigate

the evolution of the IR properties when considering fullerene–  $S_8$  co-crystals.

The PBE IR spectra of C<sub>60</sub>-2S<sub>8</sub> and C<sub>70</sub>-2S<sub>8</sub> co-crystals along with those of the isolated C<sub>60</sub> and C<sub>70</sub> molecules are displayed in Fig. 3. We note that the PBE/6-31G(d,p) and B3LYP/ 6-31G(d,p) calculations yield similar results for the investigated systems, as shown in Fig. S2 and S3 (ESI‡). As illustrated in Fig. 3, the IR spectra of both  $C_{60}$ – $2S_8$  and  $C_{70}$ – $2S_8$  co-crystals resemble very closely the spectra of  $C_{60}$  and  $C_{70}$  molecules, respectively. Some doublings of the peaks seen at high energies in Fig. 3 are due to the presence of translationally inequivalent fullerene molecules in the unit cell. Overall, the IR results are consistent with the fact that there is only negligible charge transfer between fullerene and S<sub>8</sub> molecules in the ground state and that the intermolecular interactions are entirely driven by weak van der Waals forces. This conclusion is also supported by experimental data<sup>58,59</sup> showing that the IR spectra of the C<sub>60</sub>-2S<sub>8</sub> and C<sub>70</sub>-2S<sub>8</sub> films are very similar to the spectra of the related fullerene molecules. Thus, we expect that the C<sub>60</sub>-2S<sub>8</sub> and C<sub>70</sub>-2S<sub>8</sub> co-crystals, as is the case for the C<sub>60</sub> and C<sub>70</sub> films, are potential candidates as IR imaging materials in both LWIR and MWIR windows.

#### **Optical properties**

We now turn to the optical properties of the  $C_{60}$ – $2S_8$  and  $C_{70}$ – $2S_8$  co-crystals. Here, in order to estimate the lowest excited-state energies of the systems, we performed TD-DFT calculations at the B3LYP/6-31G(d,p) level based on fullerene– $S_8$  complexes extracted from the crystal structures and consisting of one fullerene molecule and one  $S_8$  molecule. The calculated transition energies of the lowest singlet states of the  $C_{60}$ – $S_8$  and  $C_{70}$ – $S_8$  complexes are presented in Table S4 (ESI‡); selected transitions of interest in the  $C_{60}$ – $S_8$  complex along with the transition energies in the isolated molecules are also collected in Table 3.

The TD-DFT/B3LYP results highlight that the energies of the lowest 15 excited states of  $C_{60}$ – $S_8$  are identical to those of  $C_{60}$  itself. However, the energy of the next ( $S_0 \rightarrow S_{16}$ ) transition in

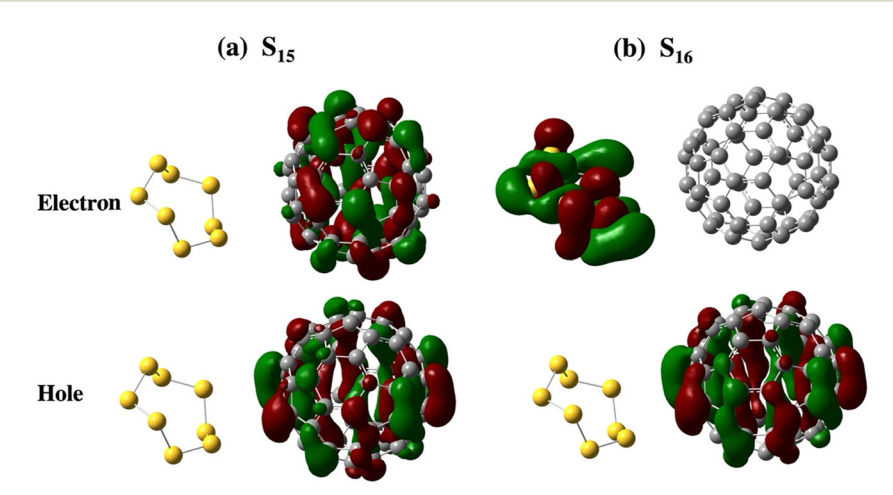


Fig. 4 Comparison of the B3LYP/6-31G(d,p) natural transition orbitals (NTOs) in the  $C_{60}$ -2S<sub>8</sub> complex between (a) the  $C_{60}$  singlet local excited state  $S_{15}$  ( $\lambda$  value for the NTO shown is 0.67; the other relevant NTOs involve additional fullerene frontier molecular orbitals) and (b) the lowest singlet charge-transfer state ( $\lambda$ (NTO) = 0.99), i.e., the  $S_{16}$  state.

the complex is lower than the corresponding transition in C<sub>60</sub> and the energy of the first excited state of S<sub>8</sub>. This clearly indicates that the S<sub>16</sub> excited state in the complex is due to interactions between C<sub>60</sub> and S<sub>8</sub> molecules. The natural transition orbitals shown in Fig. 4 indeed point to the  $S_0 \rightarrow S_{16}$ transition in the co-crystal as representing a charge-transfer transition with an electron being transferred from C<sub>60</sub> to  $S_8$ . A similar situation is found for the  $C_{70}$ – $2S_8$  co-crystal, see Table S4 and Fig. S4 (ESI‡). Thus, in both co-crystals, the lowest excited states are dominated by transitions localized on the fullerene molecules. A similar nature of the CT states is also obtained by means of TD-DFT LC-ωHPBE calculations (see Fig. S5 and Table S5, ESI‡). This finding is supported by the experimental data showing that the optical spectra of the co-crystals are similar to those of the pure fullerenes and exhibit just an additional marginal transition above the optical edge of the fullerene bands.<sup>79</sup>

### 4. Conclusions

We performed DFT calculations to investigate the charge transport, vibrational, and optical properties of the C<sub>60</sub>-2S<sub>8</sub> and C<sub>70</sub>-2S<sub>8</sub> co-crystals. DFT calculations on the crystals, fullerene-S<sub>8</sub> complexes, and the individual molecules demonstrate that all these properties are dominated by the fullerene component.

With regard to charge transport, the presence of the S<sub>8</sub> molecules does not contribute to, but also does not affect the properties of both holes and electrons in the co-crystals, with transport taking place over the networks of fullerene molecules. Interestingly, small effective masses are found for holes and electrons in both co-crystals with transport displaying a 3D character in the case of electrons.

Our calculations also show that there exist only weak van der Waals interactions between the fullerene and S<sub>8</sub> molecules in both co-crystals; in agreement with experimental data, the calculated IR spectra of the co-crystals essentially represent a simple superposition of the individual spectra of S<sub>8</sub> and fullerene molecules. Our results also suggest that fullerene-S<sub>8</sub> co-crystals could be potential candidates for thermal LWIR and MWIR imaging applications.

In terms of the optical properties, it is found that the chargetransfer transitions in both C<sub>60</sub>-2S<sub>8</sub> and C<sub>70</sub>-2S<sub>8</sub> co-crystals are located above the lowest excited states of the fullerenes. Thus, given that the first excited state in the S<sub>8</sub> molecule has a very high energy, the low-energy part of the optical spectra in the fullerene-S<sub>8</sub> co-crystals are dominated by transitions within the fullerene component.

Finally, our results indicate that, due to its optical transparency over a large energy window and the simplicity of its vibrational spectrum, an S<sub>8</sub> matrix could be used to test the effect of a solid-state environment on the intramolecular properties of various molecules and molecular complexes.

## Conflicts of interest

There are no conflicts to declare.

## Acknowledgements

This work was funded by the National Science Foundation and the Air Force Research Laboratory through DMREF-2118578 and by the College of Science of the University of Arizona. The authors are thankful for the use of the High Performance Computing (HPC) resources supported by the University of Arizona TRIF, UITS, and Research, Innovation, and Impact (RII) Offices and maintained by the Research Technologies Department.

## References

- 1 T. S. Kleine, R. S. Glass, D. L. Lichtenberger, M. E. Mackay, K. Char, R. A. Norwood and J. Pyun, 100th Anniversary of Macromolecular Science Viewpoint: High Refractive Index Polymers from Elemental Sulfur for Infrared Thermal Imaging and Optics, ACS Macro Lett., 2020, 9(2), 245-259.
- 2 J. J. Griebel, S. Namnabat, E. T. Kim, R. Himmelhuber, D. H. Moronta, W. J. Chung, A. G. Simmonds, K. J. Kim, J. Van Der Laan and N. A. Nguyen, New infrared transmitting material via inverse vulcanization of elemental sulfur to prepare high refractive index polymers, Adv. Mater., 2014, 26(19), 3014-3018.
- 3 P. T. Dirlam, J. Park, A. G. Simmonds, K. Domanik, C. B. Arrington, J. L. Schaefer, V. P. Oleshko, T. S. Kleine, K. Char and R. S. Glass, Elemental sulfur and molybdenum disulfide composites for Li-S batteries with long cycle life and high-rate capability, ACS Appl. Mater. Interfaces, 2016, 8(21), 13437-13448.
- 4 X. Ji, K. T. Lee and L. F. Nazar, A highly ordered nanostructured carbon-sulphur cathode for lithium-sulphur batteries, Nat. Mater., 2009, 8(6), 500-506.
- 5 D. Wang, Z. Tang, R. Huang, Y. Duan, S. Wu, B. Guo and L. Zhang, Interface Coupling in Rubber/Carbon Black Composites toward Superior Energy-Saving Capability Enabled by Amino-Functionalized Polysulfide, Chem. Mater., 2022, 35(2), 764-772.
- 6 S. J. Tonkin, C. T. Gibson, J. A. Campbell, D. A. Lewis, A. Karton, T. Hasell and J. M. Chalker, Chemically induced repair, adhesion, and recycling of polymers made by inverse vulcanization, Chem. Sci., 2020, 11(21), 5537-5546.
- 7 T.-J. Yue, L.-Y. Wang and W.-M. Ren, The synthesis of degradable sulfur-containing polymers: precise control of structure and stereochemistry, Polym. Chem., 2021, 12(46), 6650-6666.
- 8 M. Mann, B. Zhang, S. J. Tonkin, C. T. Gibson, Z. Jia, T. Hasell and J. M. Chalker, Processes for coating surfaces with a copolymer made from sulfur and dicyclopentadiene, Polym. Chem., 2022, 13(10), 1320-1327.
- 9 M. Mann, J. E. Kruger, F. Andari, J. McErlean, J. R. Gascooke, J. A. Smith, M. J. Worthington, C. C. McKinley, J. A. Campbell and D. A. Lewis, Sulfur polymer composites as controlled-release fertilisers, Org. Biomol. Chem., 2019, 17(7), 1929-1936.

- 10 J. M. Chalker, M. Mann, M. J. Worthington and L. J. Esdaile, Polymers made by inverse vulcanization for use as mercury sorbents, Org. Mater., 2021, 3(02), 362-373.
- 11 J. Lim, J. Pyun and K. Char, Recent approaches for the direct use of elemental sulfur in the synthesis and processing of advanced materials, Angew. Chem., Int. Ed., 2015, 54(11), 3249-3258.
- 12 W. J. Chung, J. J. Griebel, E. T. Kim, H. Yoon, A. G. Simmonds, H. J. Ji, P. T. Dirlam, R. S. Glass, J. J. Wie and N. A. Nguyen, The use of elemental sulfur as an alternative feedstock for polymeric materials, Nat. Chem., 2013, 5(6), 518-524.
- 13 R. Steudel, Liquid Sulfur, Top. Curr. Chem., 2003, 230, 81-116.
- 14 L. Liu, Y. Kono, C. Kenney-Benson, W. Yang, Y. Bi and G. Shen, Chain Breakage in Liquid Sulfur at High Pressures and High Temperatures, Phys. Rev. B: Condens. Matter Mater. Phys., 2014, 89(17), 174201.
- 15 L. Zhang, Y. Ren, X. Liu, F. Han, K. Evans-Lutterodt, H. Wang, Y. He, J. Wang, Y. Zhao and W. Yang, Chain Breakage in the Supercooled Liquid - Liquid Transition and Re-entry of the λ-transition in Sulfur, Sci. Rep., 2018, 8(1), 4558.
- 16 L. Henry, M. Mezouar, G. Garbarino, D. Sifré, G. Weck and F. Datchi, Liquid-Liquid Transition and Critical Point in Sulfur, Nature, 2020, 584(7821), 382-386.
- 17 R. E. Powell and H. Eyring, The Properties of Liquid Sulfur, J. Am. Chem. Soc., 1943, 65(4), 648-654.
- 18 M. Schmidt, Elemental Sulfur-A Challenge to Theory and Practice, Angew. Chem., Int. Ed. Engl., 1973, 12(6), 445-455.
- 19 B. Meyer, Elemental Sulfur, Chem. Rev., 1976, 76(3), 367-388.
- 20 R. Steudel, B. Eckert, Y. Steudel and M. W. Wong, Elemental Sulfur and Sulfur-Rich Compounds I, Top. Curr. Chem., 2003, 230, 1-134.
- 21 B. Meyer, M. Gouterman, D. Jensen, T. Oommen, K. Spitzer and T. Stroyer-Hansen, The spectrum of sulfur and its allotropes, ACS Publications, 1972.
- 22 S. C. Abrahams, The crystal and molecular structure of orthorhombic sulfur, Acta Crystallogr., 1955, 8(11), 661-671.
- 23 M.-T. Hao, C.-F. Du, C.-B. Tian, J.-R. Li and X.-Y. Huang, [Fe (SCN) 2 (bipy) 2]-2 (S8): A two-dimensional coordination polymer intercalating the S8 molecules, Inorg. Chem. Commun., 2016, 72, 128-131.
- 24 F. A. Cotton, P. A. Kibala and R. B. Sandor, Structural characterization of WCl6. S8, Acta Crystallogr., Sect. C: Cryst. Struct. Commun., 1989, 45(9), 1287-1289.
- 25 K. B. Ghiassi, S. Y. Chen, J. Wescott, A. L. Balch and M. M. Olmstead, New insights into the structural complexity of C60·2S8: Two crystal morphologies, two phase changes, four polymorphs, Cryst. Growth Des., 2015, 15(1), 404-410.
- 26 H. Allouchi, D. O. López, M. F. Gardette, J. L. Tamarit, V. Agafonov, H. Szwarc and R. Céolin, Thermal and mechanical behaviour of the C60·2S8 monoclinic compound, Chem. Phys. Lett., 2000, 317(1-2), 40-44.
- 27 W. Baratta, F. Calderazzo and L. M. Daniels, cyclo-Octasulfur Adducts of WCl4(S)(THF) and WCl6. Crystal and Molecular Structure of WCl4(S)(THF)·S8, Inorg. Chem., 1994, 33(17), 3842-3844.

- 28 T. Bjorvatten, O. Hassel and A. Lindheim, Crystal Structure of the Addition Compound SbI3: 3 S8, Acta Chem. Scand., 1963, 17, 689-702.
- 29 L. I. Buravov, O. A. D'Yachenko, S. V. Konovalikhin, N. D. Kushch, I. P. Lavrent'ev, N. G. Spitsyna, G. V. Shilov and E. B. Yagubskii, A complex of buckminsterfullerene with sulfur, C60·2S8: synthesis and crystal structure, Russ. Chem. Bull., 1994, 43(2), 240-244.
- 30 F. A. Cotton, P. A. Kibala and R. B. W. Sandor, Structural Characterization of WCl6·S8, Acta Crystallogr., 1989, 1287-1289.
- 31 W. S. Fernando, Single crystal Raman spectra of SbI3·3S8; CHI3· 3S8 and AsI3·3S8, J. Inorg. Nucl. Chem., 1981, 43(6), 1141-1145.
- 32 K. B. Ghiassi, S. Y. Chen, J. Wescott, A. L. Balch and M. M. Olmstead, New insights into the structural complexity of C60.2S8: Two crystal morphologies, two phase changes, four polymorphs, Cryst. Growth Des., 2015, 15(1), 404-410.
- 33 J. F. Kelly, A. Samoc, M. Samoc, E. R. Krausz and A. C. Willis, Anisotropy of second-order nonlinear optical susceptibilof arsenic triiodide-sulfur addition complex: AsI3···3S8, Opt. Commun., 2006, 264(1), 35-44.
- 34 R. Laitinen, J. Steidel and R. Steudel, The Crystal Structures and Raman Spectra of 2S8.SnI4 and 2S(n)Se(8-n).SnI4, Acta Chem. Scand., 1980, 34A, 687-693.
- 35 G. A. Marking and M. G. Kanatzidis, Encapsulation of Cyclooctasulfur Molecules in an Open Metal-Sulfide Framework. Isolation of the Host-Guest Complex Cs2Sn3S7·1/2S8 from Molten Cesium Polysulfide Fluxes, Chem. Mater., 1995, 7(10), 1915-1921.
- 36 R. H. Michel, M. M. Kappes, P. Adelmann and G. Roth, Preparation and Structure of C76(S8)6: A First Step in the Crystallographic Investigation of Higher Fullerenes, Angew. Chem., Int. Ed. Engl., 1994, 33(15-16), 1651-1654.
- 37 H. W. Kroto, J. R. Heath, S. C. O'Brien, R. F. Curl and R. E. Smalley, C60: Buckminsterfullerene, Nature, 1985, **318**(6042), 162–163.
- 38 R. C. Haddon, A. F. Hebard, M. J. Rosseinsky, D. W. Murphy, S. J. Duclos, K. B. Lyons, B. Miller, J. M. Rosamilia, R. M. Fleming, A. R. Kortan, S. H. Glarum, A. V. Makhija, A. J. Muller, R. H. Eick, S. M. Zahurak, R. Tycko, G. Dabbagh and F. A. Thiel, Conducting Films of C60 and C70 by Alkali-Metal Doping, Nature, 1991, 350(6316), 320-322.
- 39 V. N. Sathiyamoorthy, H. Mizuseki and Y. Kawazoe, Hydrogen Storage on Nanofullerene Cages, NANO, 2009, 04(05), 253-263.
- 40 S. S. Han, J. L. Mendoza-Cortés and W. A. Goddard Iii, Recent Advances on Simulation and Theory of Hydrogen Storage in Metal-Organic Frameworks and Covalent Organic Frameworks, Chem. Soc. Rev., 2009, 38(5), 1460-1476.
- 41 S. Goodarzi, T. Da Ros, J. Conde, F. Sefat and M. Mozafari, Fullerene: Biomedical Engineers Get to Revisit an Old Friend, Mater. Today, 2017, 20(8), 460-480.
- 42 H. Yin, H. Lin, Y. Zong and X.-D. Wang, The Recent Advances in C60 Micro/Nanostructures and their Optoelectronic Applications, Org. Electron., 2021, 93, 106142.

- 43 M. Makha, A. Purich, C. L. Raston and A. N. Sobolev, Structural diversity of host-guest and intercalation complexes of fullerene C60, *Eur. J. Inorg. Chem.*, 2006, (3), 507–517.
- 44 J. Yang, P. Sullivan, S. Schumann, I. Hancox and T. S. Jones, Organic photovoltaic cells based on unconventional electron donor fullerene and electron acceptor copper hexadecafluorophthalocyanine, *Appl. Phys. Lett.*, 2012, 100(2), 023307.
- 45 T. Zhuang, X.-F. Wang, T. Sano, Z. Hong, G. Li, Y. Yang and J. Kido, Fullerene C70 as a p-type donor in organic photovoltaic cells, *Appl. Phys. Lett.*, 2014, **105**(9), 093301.
- 46 Z. Xing, F. Liu, S. H. Li, X. Huang, A. Fan, Q. Huang and S. Yang, Bowl-Assisted Ball Assembly for Solvent-Processing the C60 Electron Transport Layer of High-Performance Inverted Perovskite Solar Cell, *Angew. Chem., Int. Ed.*, 2023, 62(34), e202305357.
- 47 G. Wetzelaer, Trap-free space-charge-limited hole transport in a fullerene derivative, *Phys. Rev. Appl.*, 2019, **11**(2), 024069.
- 48 T. D. Anthopoulos, C. Tanase, S. Setayesh, E. J. Meijer, J. C. Hummelen, P. W. M. Blom and D. de Leeuw, Ambipolar organic field-effect transistors based on a solution-processed methanofullerene, *Adv. Mater.*, 2004, **16**(23–24), 2174–2179.
- 49 E. Cho, V. Coropceanu and J.-L. Brédas, Hole versus electron transport in fullerenes, *Org. Electron.*, 2023, **118**, 106798.
- 50 J. Gong, Y. Li, S. Lin, G. Ma, Y. Yang and G. Chen, Enhancement of electrical conductivity in sulfur-doped C60 films, *Thin Solid Films*, 1997, 302(1), 256–259.
- 51 H. Allouchi, D. López, M.-F. Gardette, J. L. Tamarit, V. Agafonov, H. Szwarc and R. Céolin, Thermal and mechanical behaviour of the C60· 2S8 monoclinic compound, *Chem. Phys. Lett.*, 2000, 317(1–2), 40–44.
- 52 H. Takahashi, E. Matsubara, M. Shiro, S. Matsubara, N. Sato, A. Muramatsu and K. Tohji, Co-deposition of fullerenes and sulfur from diluted solution, *Fullerenes, Nano*tubes Carbon Nanostruct., 2002, 10(3), 217–226.
- 53 G. Roth and P. Adelmann, Preparation and crystal structure of C 60 S 16, *Appl. Phys. A: Solids Surf.*, 1993, **56**, 169–174.
- 54 R. H. Michel, M. M. Kappes, P. Adelmann and G. Roth, Preparation and structure of C76 (S8) 6: A first step in the crystallographic investigation of higher fullerenes, *Angew. Chem., Int. Ed. Engl.*, 1994, 33(15–16), 1651–1654.
- 55 A.-S. Grell, F. Masin, R. Céolin, M. F. Gardette and H. Szwarc, Molecular dynamics of C 60 2 S 8: A 13 C NMR study, *Phys. Rev. B: Condens. Matter Mater. Phys.*, 2000, 62(6), 3722.
- 56 M.-F. Gardette, A. Chilouet, S. Toscani, H. Allouchi, V. Agafonov, J.-C. Rouland, H. Szwarc and R. Céolin, Phase equilibria in the C60-sulphur system, *Chem. Phys. Lett.*, 1999, **306**(3-4), 149-154.
- 57 A. V. Talyzin, L. E. Tergenius and U. Jansson, Single-crystal growth of C70S8 a new phase in the C70–sulphur system, *J. Cryst. Grow.*, 2000, **213**(1), 63–69.
- 58 A. Talyzin and U. Jansson, Preparation and characterization of C60S16 and C70S48 thin films, *Thin Solid Films*, 1999, 350(1-2), 113-118.

- 59 H. Takahashi, E. Matsubara, R. V. Belosludov, S. Matsubara, N. Sato, A. Muramatsu, Y. Kawazoe and K. Tohji, Fullerene and Sulfur Compounds, *Mater. Trans.*, 2002, 43(7), 1530–1532.
- 60 J. Xiang, W. Shen, Z. Guo, J. Meng, L. Yuan, Y. Zhang, Z. Cheng, Y. Shen, X. Lu and Y. Huang, A Supramolecular Complex of C60–S with High-Density Active Sites as a Cathode for Lithium–Sulfur Batteries, *Angew. Chem., Int. Ed.*, 2021, 60(26), 14313–14318.
- 61 L. Wang, Solvated fullerenes, a new class of carbon materials suitable for high-pressure studies: A review, *J. Phys. Chem. Solids*, 2015, **84**, 85–95.
- 62 J. Hafner, Ab-initio simulations of materials using VASP: Density-functional theory and beyond, *J. Comput. Chem.*, 2008, 29(13), 2044–2078.
- 63 J. P. Perdew, K. Burke and M. Ernzerhof, Generalized gradient approximation made simple, *Phys. Rev. Lett.*, 1996, 77(18), 3865.
- 64 G. Kresse and J. Furthmüller, Efficient iterative schemes for ab initio total-energy calculations using a plane-wave basis set, *Phys. Rev. B: Condens. Matter Mater. Phys.*, 1996, 54(16), 11169.
- 65 X. Wu, D. Vanderbilt and D. Hamann, Systematic treatment of displacements, strains, and electric fields in density-functional perturbation theory, *Phys. Rev. B: Condens. Matter Mater. Phys.*, 2005, 72(3), 035105.
- 66 D. Karhanek, *Self-assembled monolayers studied by density-functional theory*, 2010, PhD thesis, University of Vienna.
- 67 E. F. Valeev, V. Coropceanu, D. A. Da Silva Filho, S. Salman and J.-L. Brédas, Effect of Electronic Polarization on Charge-Transport Parameters in Molecular Organic Semiconductors, *J. Am. Chem. Soc.*, 2006, 128(30), 9882–9886.
- 68 Y. Yi, V. Coropceanu and J.-L. Brédas, Nonlocal Electron-Phonon Coupling in the Pentacene Crystal: Beyond the *Γ*-Point Approximation, *J. Chem. Phys.*, 2012, **137**(16), 164303.
- 69 E. Cho, V. Coropceanu and J.-L. Brédas, Electronic Structure of Multicomponent Organic Molecular Materials: Evaluation of Range-Separated Hybrid Functionals, *J. Chem. Theory Comput.*, 2020, 16(6), 3712–3719.
- 70 A. Donaldson and A. Caplin, Refractive index of molten sulphur, *Philos. Mag. B*, 1985, **52**(2), 185–197.
- 71 S. Sami, P. A. Haase, R. Alessandri, R. Broer and R. W. Havenith, Can the dielectric constant of fullerene derivatives be enhanced by side-chain manipulation? A predictive first-principles computational study, *J. Phys. Chem. A*, 2018, **122**(15), 3919–3926.
- 72 M. Frisch, G. Trucks, H. B. Schlegel, G. Scuseria, M. Robb, J. Cheeseman, G. Scalmani, V. Barone, G. Petersson and H. Nakatsuji, *Gaussian* 16, Gaussian, Inc., Wallingford, CT, 2016.
- 73 S. Saito and A. Oshiyama, Cohesive mechanism and energy bands of solid, *Phys. Rev. Lett.*, 1991, **66**(20), 2637–2640.
- 74 W. J. Chung, J. J. Griebel, E. T. Kim, H. Yoon, A. G. Simmonds, H. J. Ji, P. T. Dirlam, R. S. Glass, J. J. Wie, N. A. Nguyen, B. W. Guralnick, J. Park, Á. Somogyi, P. Theato, M. E. Mackay, Y.-E. Sung, K. Char and J. Pyun, The Use of Elemental Sulfur as an Alternative Feedstock for Polymeric Materials, *Nat. Chem.*, 2013, 5(6), 518–524.
- 75 J. J. Griebel, S. Namnabat, E. T. Kim, R. Himmelhuber, D. H. Moronta, W. J. Chung, A. G. Simmonds, K.-J. Kim,

- J. van der Laan, N. A. Nguyen, E. L. Dereniak, M. E. Mackay, K. Char, R. S. Glass, R. A. Norwood and J. Pyun, New Infrared Transmitting Material via Inverse Vulcanization of Elemental Sulfur to Prepare High Refractive Index Polymers, Adv. Mater., 2014, 26(19), 3014-3018.
- 76 T. Lee, P. T. Dirlam, J. T. Njardarson, R. S. Glass and J. Pyun, Polymerizations with Elemental Sulfur: From Petroleum Refining to Polymeric Materials, J. Am. Chem. Soc., 2022, 144(1), 5-22.
- 77 R. Steudel, Elemental sulfur and sulfur-rich compounds II, Springer Science & Business Media, 2003, vol. 2.
- 78 E. Cho, S. M. Pratik, J. Pyun, V. Coropceanu and J.-L. Brédas, π-Conjugated Carbon-Based Materials for Infrared Thermal Imaging, Adv. Opt. Mater., 2023, 11(12), 2300029.
- 79 N. D. Kushch, I. Majchrzak, W. Ciesielski, A. Graja, K. Woźniak and T. M. Krygowski, New sulfur-fullerite; its preparation, structure and spectral properties, J. Phys., 1993, 3(10), 1987-1991.